### Title

Rapid Stoichiometry Control in Cu2Se Thin Films for Room-Temperature Power Factor Improvement




### Journal

ACS Applied Energy Materials, 2(2)

### ISSN

2574-0962



### Authors

Scimeca, Michael R
Yang, Fan
Zaia, Edmond
et al.



### Publication Date

2019-02-25

### DOI

10.1021/acsaem.8b02118

Peer reviewed

# Rapid Stoichiometry Control in $Cu_2Se$ Thin Films for Room-Temperature Power Factor Improvement

Michael R. Scimeca,[†] Fan Yang,[‡,§] Edmond Zaia,[‡,∥] Nan Chen,[†] Peter Zhao,[†,⊥] Madeleine P. Gordon,[‡,#] Jason D. Forster,[‡] Yi-Sheng Liu,[¶] Jinghua Guo,[¶] Jeffrey J. Urban,[*,‡] and Ayaskanta Sahu[*,†]

[†]Department of Chemical and Biomolecular Engineering, NYU Tandon School of Engineering, Brooklyn, New York 11201, United States

[‡]The Molecular Foundry, Lawrence Berkeley National Laboratory, Berkeley, California 94720, United States

[§]Department of Mechanical Engineering, Stevens Institute of Technology, Hoboken, New Jersey 07030, United States

[∥]Department of Chemical and Biomolecular Engineering, University of California, Berkeley, California 94720, United States

[⊥]Department of Chemical Engineering, Cooper Union, New York, New York 10003, United States

[#]Applied Science and Technology Graduate Group, University of California, Berkeley, California 94720, United States

[¶]Advanced Light Source, Lawrence Berkeley National Laboratory, Berkeley, California 94720, United States

**ABSTRACT:** $Cu_2Se$ thin films provide a promising route toward relatively safe, sustainable and solution processed thermoelectric (TE) modules in contrast to more expensive and toxic materials currently on the market such as $Bi_2Te_3$. $Cu_2Se$ is known in the TE community for its high performance at high temperature and has recently attracted attention from its large theoretically predicted figure of merit at room temperature. Unfortunately, one of the main limitations encountered so far in $Cu_2Se$ thin films is that the carrier concentrations are not optimized for TE operation after solution processing. In this work, we conduct a comprehensive study of the structural, optical, and TE properties of $Cu_2Se$ thin films and demonstrate that nonoptimized carrier concentrations in these films lead to observations of poor performance at room temperature. Through a simple soaking procedure in a $Cu^+$ ion solution for only a few minutes, we demonstrate a 200−300% increase in power factor. This soaking process pushes the carrier concentration of the $Cu_2Se$ thin film toward its optimal value for TE operation and marks the highest TE performance for any solution processed $Cu_2Se$ thin film at room temperature thus far. If the performance can be further optimized at room temperature, $Cu_2Se$ thin films will be the material of choice to utilize in TE modules for powering miniature electronics and sensors, which has been an increasingly popular and rapidly expanding market.

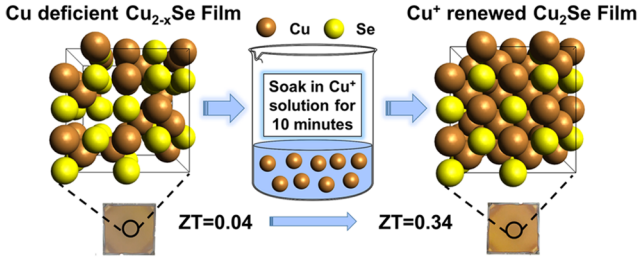


## INTRODUCTION

With a global initiative to move toward cleaner energy technologies,[1−8] thermoelectric (TE) devices, which can directly convert thermal energy into electrical energy and vice versa have the unique advantage of providing a clean, quiet, reliable, and safe source of power generation or solid-state cooling.[9−11] Traditional refrigerants possessing potent greenhouse gases can be replaced with the implementation of TE solid state cooling technology.[12] In addition, the emergence of wearable microelectronics[13−18] creates inspiration for flexible TE power generation and cooling devices that can be integrated into clothing.[19,20]

To gauge the efficiency of a TE material, the figure of merit, $ZT = \frac{\alpha^2\sigma}{\kappa}T$, and power factor, $\alpha^2\sigma$, are two commonly used performance indicators, where $\alpha$ is the Seebeck coefficient, $\sigma$ is the electrical conductivity, $\kappa$ is the total thermal conductivity from electron and phonon contributions, and $T$ is the absolute temperature of the material.[21] To achieve a high $ZT$, a TE material needs to simultaneously exhibit a high Seebeck coefficient, high electrical conductivity, and low thermal conductivity. Improving $ZT$ is difficult because these parameters ($\alpha$, $\kappa$, and $\sigma$) are interrelated and thermal conductivity typically increases with electrical conductivity.[7] Strategies to break these relationships in materials have traditionally involved nanostructuring and energy filtering.[22−26] While $ZT$ values focus simply on the material potential of a TE material, cost-effective processability, and sustainability should also be considered. At a

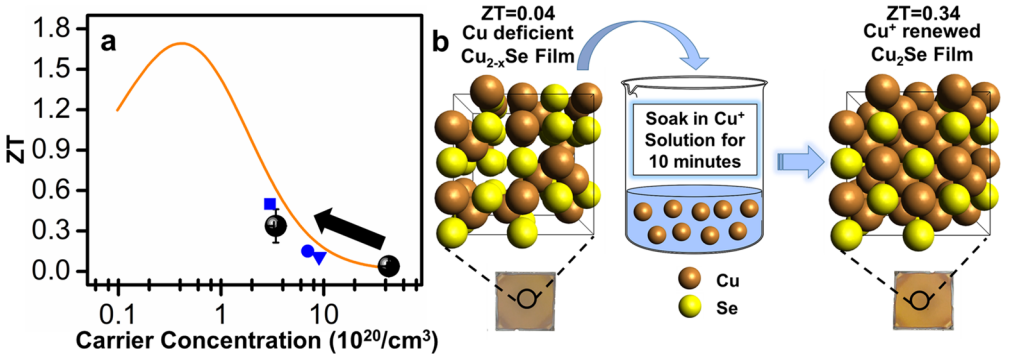


**Figure 1.** (a) Theoretically calculated TE figure of merit, $ZT$, as a function of carrier concentration at $T = 305$ K. Values of the parameters input into the model are from literature: effective mass, $m^* = 3.15m_e$[56] ($m_e$ is defined as the mass of an electron at rest), lattice perturbation constant, $\mu_0 = 34$ cm$^2$/(V s)[32] and lattice thermal conductivity, $\kappa_{lat} = 0.16$ W/mK.[32] $\kappa_{elec}$ is calculated based on the Wiedemann–Franz law. Experimental values of $ZT$ (black spheres) are plotted in addition to other published results for comparison: blue triangle,[21] blue circle,[20] and blue square.[58] (b) Cartoon depicting the strategy to remove Cu deficiency in $Cu_{2-x}Se$ thin films samples by soaking in a solution of Cu ions. Cu ions are kinetically driven into the $Cu_{2-x}Se$ crystal lattice and fill in any Cu vacancies to improve $ZT$ from 0.04 to 0.34. The photos show $Cu_2Se$ films on glass substrates.

system level, to alleviate the cost of manufacturing and to develop flexible TE devices, solution processing[12,27,28] offers the advantages of manufacturing at lower temperatures and pressures while reducing the amount of waste material.[12,21] With solution processing, flexible thin films of TE material can be fabricated at a low cost.[29] Significant advancements in the TE research community have been reported in the past few decades; however, the materials and manufacturing processes used are still either too expensive or wasteful.[11] The best materials demonstrating high $ZT$ at room temperature (typically around 1) have historically included the use of rare or toxic elements in inorganic crystalline semiconductors, such as $Bi_2Te_3$ and $Sb_2Te_3$, and fabricated using energy intensive techniques, including vacuum melting and spark plasma sintering (SPS).[12,30,31] To address these shortcomings, $Cu_2Se$ has been proposed as a relatively nontoxic and abundant alternative with theoretical predictions of a maximum bulk $ZT$ around 1.16 at 305 K.[32−34] Numerous experimental results have demonstrated promising TE performance of $Cu_2Se$, while operating at high temperature (>800 K) with a $ZT$ of around 1.5.[19,35−40] However, these high $ZT$ values are only obtained via expensive manufacturing practices.[11] Additionally, at high operating temperatures, $Cu_2Se$ demonstrates instability which would lead to degradation of performance over time.[34,41,42] At room temperature, we expect minimal degradation of $Cu_2Se$ as compared to high temperature operation. In addition, nanostructuring $Cu_2Se$ can potentially improve material stability due to limiting $Cu^+$ diffusivity at the interfaces.[43,44] The best $ZT$ values recently reported for solution processed $Cu_2Se$ at room temperature are only 0.14 in spite of predicted values of over 1.[21,32] In this Article, we show that the reason for this low performance is due to extremely high carrier concentrations in $Cu_2Se$ resulting from Cu vacancies and self-doping, which drastically affect the Seebeck coefficient. We then proceed to demonstrate a simple yet effective approach that introduces excess Cu ions into the $Cu_2Se$ lattice, fills in the vacancies, and leads to about 200−300% improvements in as-synthesized $Cu_2Se$ thin films.

## BACKGROUND

The most direct and ideal route to solution processed semiconductor materials would be to dissolve them in a solvent, deposit on any substrate and anneal to remove the solvent. However, crystalline semiconductors are typically insoluble in most common solvents. One solvent that has had success dissolving these materials is hydrazine.[45−48] Unfortunately, hydrazine is a poor option for large applications due to its explosive and toxic properties.[12] Recently, Webber et al. developed a method to completely dissolve metal chalcogenides, including $Cu_2Se$, into a thiol-amine solution.[49−51] This binary solvent combination has the advantage of being less dangerous than hydrazine,[12] and the deposition of metal chalcogenides using this technique yields closely packed, void-free thin films without the need for spark plasma sintering or hot pressing.[11] The close contact of each crystalline grain within the thin film should lead to improved electron transport and an improved power factor in TE devices. With the apparent success of this facile metal chalcogenide fabrication process, our overall goal is to match and even exceed the TE performance achieved from higher cost fabrication processes. If achieved, this result would lead to massive cost savings and pave the way for environmentally friendly, high performance TE devices to be deployed on a commercial scale.

A power factor of 2000 $\mu$W/(m*K$^2$) would result in a $ZT$ of 1 assuming our measured thermal conductivity of 0.6 W/(m K) at room temperature. Currently, room temperature power factors of $Cu_2Se$ materials fabricated using the cosolvent thiol-amine solution range widely from 80 to 180 $\mu$W/(m K$^2$) depending on annealing temperature.[11,12] Typically, $Cu_2Se$ exhibits p-type behavior and has a hole concentration range between $10^{20}$ to $10^{22}$ 1/cm$^3$.[20] Large discrepancies in the reported power factors and carrier concentrations in $Cu_2Se$ stem from different synthesis protocols that produce samples with varying degrees of nonstoichiometry and carrier concentrations as seen in Figure 1a.[11,12,21] Off stoichiometry is stable in $Cu_2Se$ and Cu deficiency can even reach $Cu_{1.7}Se$.[12,21] Cu deficiency is also known to create an equivalent concentration of hole carriers[19] which leads to a high hole carrier concentration in $Cu_2Se$. Even though most reports refer to the as-synthesized products as $Cu_2Se$, the products are very likely to be $Cu_{2-x}Se$, where the carrier concentration heavily depends on $x$.[21,52] For example, changing $x$ from 0.28 to 0.01 can change the carrier concentration more than an order of magnitude from $4 \times 10^{21}$ to $2 \times 10^{20}$ 1/cm$^3$ assuming carrier concentration is directly proportional to Cu deficiency.[21,52] To further improve the power factor, one can tune the carrier concentration of these $Cu_2Se$ thin films as demonstrated in similar systems, such as $Ag_2Se$, where an excess of Se was provided to reduce the amount of electrons, and $Cu_2S$,

where the stoichiometry was tuned from $Cu_{1.97}S$ to $Cu_2S$ to optimize the power factor.[12,53−55] We simulate the expected $ZT$ as a function of carrier concentration using material parameters[32,49,56,57] from literature and observe that if the carrier concentration can be reduced to $4 \times 10^{19}$ 1/cm$^3$, $ZT$ can be improved to 1.69 at room temperature (Figure 1a).[20,32]

The details of this calculation are presented in the Supporting Information (SI). Elemental doping and modulating off-stoichiometry have been implemented to tune carrier concentrations in $Cu_2Se$.[20,32] For instance, Day et al., achieved only a marginal improvement of 33% in $ZT$ in $Cu_2Se$ by doping with Br.[32] Our approach relies on reducing the number of Cu vacancies in the system by reinfusing the $Cu_2Se$ lattice with Cu ions using a technique adapted from the Manna group,[59−61] which pushes the carrier concentration closer to the optimal value of $4 \times 10^{19}$ 1/cm$^3$.[32] Our results show a nearly 300% increase in power factor from 168 to 653 $\mu$W/(m K$^2$) by simply soaking an annealed $Cu_2Se$ thin film in a solution of Cu ions for 7 min at room temperature. To the best of our knowledge, this value is the highest power factor for a solution processed $Cu_2Se$ thin film reported at room temperature.

## RESULTS AND DISCUSSION

As shown in Figure 1b, we propose that soaking a $Cu_{2-x}Se$ thin film in a solution of Cu ions creates a large Cu concentration gradient where it is energetically favorable for Cu ions to be kinetically driven into the $Cu_{2-x}Se$ lattice to fill vacancies and decrease the carrier concentration. This technique was initially employed to reduce $Cu_{2-x}Se$ nanocrystals into stoichiometric $Cu_2Se$ nanocrystals for a cation exchange experiment.[61] Since nanocrystals have a high surface area to volume ratio, the Cu ions do not have to diffuse long distances and can efficiently fill in vacancies. For our thin films, this method works since we are working with nanosized $Cu_2Se$ grains (on the order of 40 nm, Figure 2).

The ability to tune carrier concentrations through this simple Cu ion infusion technique results in a competitive advantage for nanostructured materials as compared to bulk materials. To test this hypothesis, bulk $Cu_2Se$ powder was first dissolved into a thiol-amine mixture to get a stable suspension as shown in Figure S1a and then a thin layer of $Cu_2Se$ was spin-coated onto a glass substrate (Figure S1b). Scanning electron microscope (SEM) images presented in Figures 2a and 2b show the quality of the deposited films which can be tuned by changing the concentration of the starting solution and/or deposition conditions. As-deposited films are then soaked in a 0.05 M tetrakis(acetonitrile)copper(I)hexafluorophosphate ($[Cu(CH_3CN)_4]PF_6$) solution in acetonitrile for different amounts of time to tune the vacancy concentration. We selected $[Cu(CH_3CN)_4]PF_6$ as the $Cu^+$ precursor because of its slow reactivity,[62] which enabled us to accurately control the addition of $Cu^+$ ions into the thin films on the time scale of minutes and ensure unintentional doping is minimized as the strong P−F bonds in the $PF_6^{3-}$ anion would prevent P or F doping in the film. Figure 2c and 2d shows SEM images of the postsoaked film revealing no discernible change in the morphology of the films. To verify that our film composition was not compromised by the soaking process, we used X-ray photoelectron spectroscopy (XPS) to detect the presence of both Cu and Se and observed no discernible change or unintentional doping in the spectra before and after soaking (Figure S2). We further examined the oxidation state of Cu in the films by performing high-resolution X-ray absorption spectroscopy (XAS) using a synchrotron

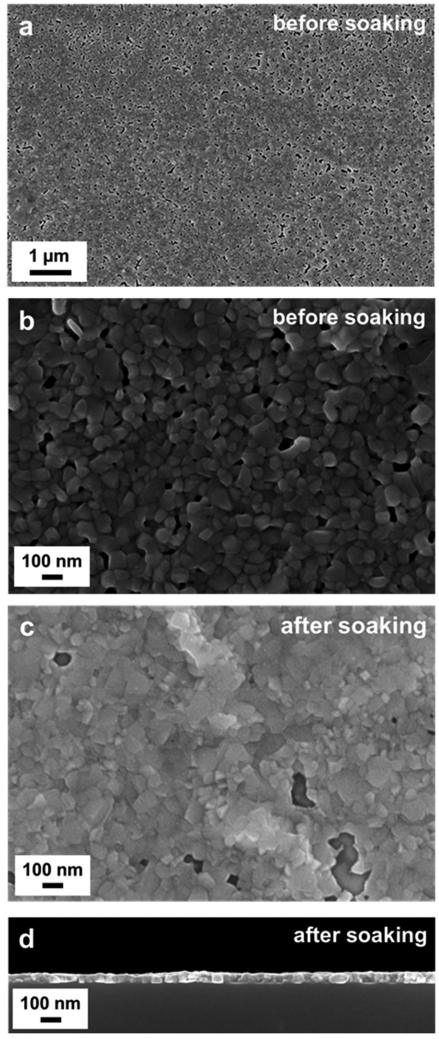


**Figure 2.** Scanning electron microscope (SEM) images of a $Cu_{2-x}Se$ thin film sample: (a, b) before soaking top view, (c) after soaking top view, and (d) after soaking cross sectional view. These images demonstrate the uniformity and thickness of the $Cu_{2-x}Se$ thin film samples.

radiation source at the Cu $L_{2,3}$-edge for 3 different samples with nominal stoichiometries of $Cu_{1.99}Se$, $Cu_{1.98}Se$, and $Cu_{1.90}Se$ (Figure S3). The spectra show $2p^{3/2}$ characteristic transitions of both $Cu^{1+}$ and $Cu^{2+}$ species at 931.5 and 929.5 eV, respectively, even in the $Cu_{1.99}Se$ sample, which could be either due to the much larger absorption cross-section for $Cu^{2+}$ than $Cu^{1+}$ species or minute amounts of $Cu^{2+}$ oxide or selenite impurities (CuO or $CuSeO_3$).[63,64]

To probe the structure further and observe if any structural changes occur in the crystal lattice of the $Cu_{2-x}Se$ thin film with a change in stoichiometry, we performed X-ray diffraction (XRD) analysis. According to the phase diagram presented by Kang et al., changes in off-stoichiometry $x$ in $Cu_{2-x}Se$ can induce structural phase transitions as well.[52] $Cu_2Se$ has two phases of interest for our application: the low-temperature $\alpha$-phase and the superionic high-temperature $\beta$-phase, where the TE properties rapidly transition.[65,66] In the $\beta$-phase, the Se atoms are positioned in a face-centered cubic arrangement and the Cu ions are disordered throughout the lattice.[58,67] The $\alpha$-phase is not fully understood but is estimated to be a mixture of layered structures, where the cations are ordered.[19,52,68] In their report,

Kang et al. argued that the transition between the $\alpha$ and $\beta$ phases is a first-order phase transition, where a phase mixture can exist near the phase boundaries.[52] At a stoichiometry of $Cu_{1.9}Se$, a two-phase mixture is often observed at room temperature which agrees well with the phase diagram.[12,52] In fact, an off stoichiometry of just $Cu_{1.97}Se$ ($x$ = 0.03) can result in the formation of the $\beta$-phase at room temperature.[69] Increasing Cu vacancies is reported to distort the structure of the $\alpha$-phase until a rearrangement to the $\beta$-phase is energetically favorable.[58] For TE applications, the $\alpha$-phase of $Cu_2Se$ is preferred because it has a lower carrier concentration than the $\beta$-phase.[52]

A dropcast thick film is used to validate the crystal structure transformation from $Cu_{2-x}Se$ to $Cu_2Se$. To directly observe structural changes before and after soaking $Cu_{2-x}Se$ films in a Cu ionic solution, XRD data sets are presented in Figure 3a, which compares XRD structural features in a $Cu_{2-x}Se$ film before and after soaking to a perfectly stoichiometric $Cu_2Se$ reference sample.

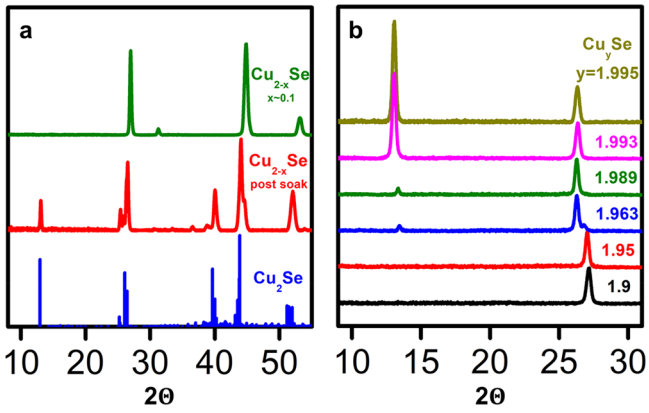


**Figure 3.** (a) Powder diffraction data for $Cu_2Se$ low temperature alpha phase (blue),[70] X-ray diffraction (XRD) data for dropcast $Cu_{2-x}Se$ samples prepared in this work with a Cu deficiency of about $x$ = 0.1 before soaking in Cu ions (green) and XRD data for $Cu_{2-x}Se$ samples after soaking in Cu ions (red). The XRD data shows there is a crystal phase transition after soaking which closely matches the $Cu_2Se$ low temperature phase reference data. (b) XRD patterns of spin-coated $Cu_2Se$ samples prepared in this work with stoichiometric compositions of $Cu_{1.9}Se$ (black), $Cu_{1.95}Se$ (red), $Cu_{1.963}Se$ (blue), $Cu_{1.989}Se$ (green), $Cu_{1.993}Se$ (pink), and $Cu_{1.995}Se$ (dark yellow). With an increasing Cu:Se ratio, a new XRD peak appears at about 13° corresponding to the (004) crystal plane and the peak at 27° corresponding to the (111) crystal plane[70] shifts to the left indicating a phase transition to the low temperature phase.

It is observed that the $\beta$-phase is the dominant phase with Cu deficient samples. After soaking, the vacancies are filled and the $\alpha$-phase dominates which is evidenced by a shift in the $2\theta$ peak of 27° toward the left to lower values of $2\theta$ and the emergence of a new peak at 13°. In addition, the XRD peaks of the postsoak sample closely resemble stoichiometric $Cu_2Se$ at a higher $2\theta$ range between 35° and 55°. At around 46°, one can observe a small peak which can be attributed to small grains of $Cu_{2-x}Se$ that were not infused with Cu ions since the film is several microns thick. After demonstrating that a crystal phase transition occurs with dropcast films, we performed XRD analysis for various stoichiometric ratios of $Cu_{2-x}Se$ using spin-coated thin films (Figure 3b) where the shorter diffusion length of the 2D films should lead to faster and more complete crystal structure transitions. As the stoichiometric ratio is improved toward $Cu_2Se$, the peak around a $2\theta$ of 27° shifts toward the left and another peak around a $2\theta$ of 13° emerges at a stoichiometry of $Cu_{1.963}Se$. These XRD trends are again representative of the $\alpha$-phase of $Cu_2Se$.[58] This corresponds well with the phase diagram which reports a phase mixture at room temperature with this stoichiometric ratio. The XRD peak intensity is proportional to the phase fraction[52] and a complete phase change from $\beta$ to $\alpha$ most likely occurs at a stoichiometry of $Cu_{1.993}Se$ with an increased intensity of the $2\theta$ peak at 13°. This complete phase change signals that this soaking technique is best suited for 100 nm thin films as compared to much thicker (1−2 $\mu$m) dropcast samples.

We obtained optical absorbance data to detect the presence and concentration of vacancies in a $Cu_{2-x}Se$ crystal lattice to better understand if and how off-stoichiometry influences the energy band diagram for a $Cu_{2-x}Se$ thin film. To clearly observe how different stoichiometric ratios affect absorbance spectra, we obtained ultraviolet−visible−near-infrared spectroscopy (UV−vis−NIR) data for six different Cu:Se ratios ranging from $Cu_{1.9}Se$ to $Cu_{1.995}Se$. To highlight the observed trend seen in the absorbance data presented in Figure 4a, we compare the lowest stoichiometric ratio with the highest stoichiometric ratio of $Cu_{2-x}Se$.

For a $Cu_{1.9}Se$ sample, we observe a sharp peak in absorbance at around a 500 nm wavelength, followed by broadband absorption at higher wavelengths (starting at 800 nm and above). For $Cu_{1.995}Se$, the narrow peak is skewed toward longer wavelengths (lower energy) and the broad absorption at higher wavelengths seen in $Cu_{1.9}Se$ disappears when the stoichiometry approaches $Cu_2Se$. The sharp peak corresponds to band-edge or interband absorption, while the broad peak at longer wavelengths corresponds to intraband absorption. We propose an explanation for this phenomenon through the energy diagram presented in Figure 4b. As $x$ increases in $Cu_{2-x}Se$, the number of Cu vacancies in the lattice increases. As vacancies increase, the chemical potential is pushed further into the valence band and there is a greater probability for electrons to exist at lower energy states away from the valence edge.[52] With empty states in the valence band, electrons can now be excited in two ways: intraband excitation and interband excitation. Intraband excitation can occur when electrons move from a lower energy state in the valence band to a higher energy state still within the valence band. If there are many available states in the valence band, there is a large range of energies that can excite an electron from one energy state to another within the band. In addition, the energy differences between states in intraband excitation are small because the states are spaced close together, and there is no bandgap to surmount. Referring to the UV−vis−NIR data, the broad, lower energy absorbance (>800 nm) can be attributed to intraband electron excitation. As for interband excitation, the amount of energy required must be large enough to raise the energy of the electron from its current state to the first available state in the conduction band. Compared to intraband excitation, interband excitation requires higher energy and is represented by the narrow peak at higher energy (<800 nm) in the UV−vis−NIR data.

As vacancies are filled, the chemical potential should rise and electrons should increasingly occupy all available states up to the valence edge. Thus, the amount of energy needed to excite an electron to the conduction band will decrease and approach the energy of the band gap while intraband excitation ought to be eliminated. This hypothesis is corroborated through the UV−vis−NIR data (Figure 4a), where the onset of the narrow

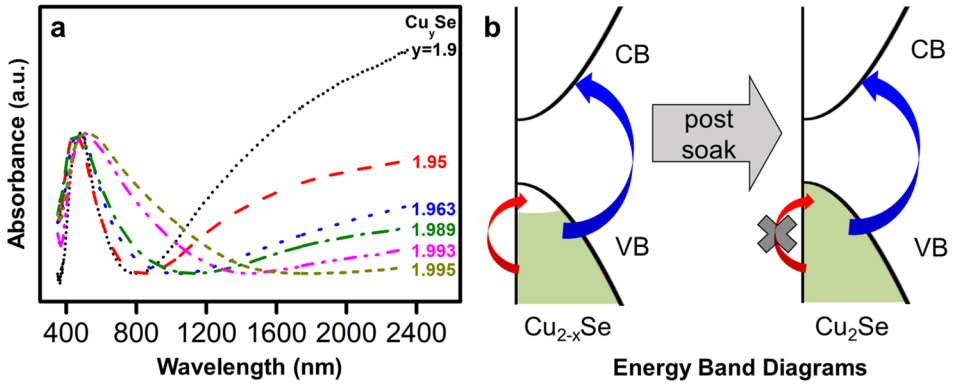


**Figure 4.** (a) Ultraviolet−visible−near-infrared spectroscopy (UV−vis−NIR) data for $Cu_2Se$ samples with various Cu deficiency levels indicated by the variable $y$: $Cu_{1.9}Se$ (black), $Cu_{1.95}Se$ (red), $Cu_{1.963}Se$ (blue), $Cu_{1.989}Se$ (green), $Cu_{1.993}Se$ (pink), and $Cu_{1.995}Se$ (dark yellow). As the stoichiometry approaches $Cu_2Se$, the short wavelength peak broadens, while the long wavelength peak is quenched suggesting changes in interband and intraband electronic transitions. (b) Cartoon depicting how electrons occupy and transition between energy levels in the conduction and valence bands for a Cu deficient sample and a perfectly stoichiometric $Cu_2Se$ sample, where $x$ represents the amount of Cu deficiency. CB represents the conduction band, while VB represents the valence band. The blue arrow depicts interband transitions while the red arrow depicts intraband transitions. The green region depicts the energy level to which electrons are filled in the VB. The intraband electronic transitions are quenched, while the minimum interband electronic transition approaches the electronic bandgap energy when Cu vacancies are filled.

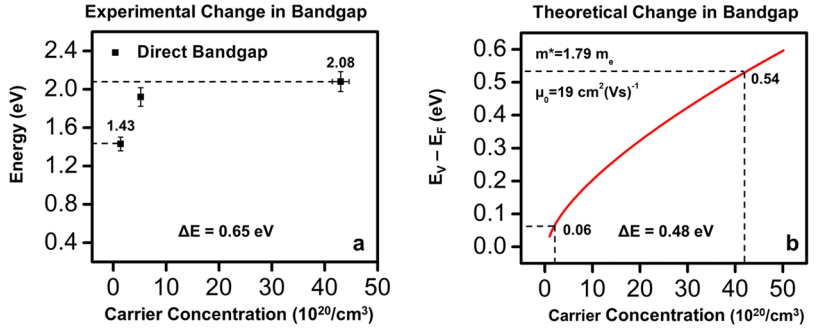


**Figure 5.** (a) Direct bandgaps calculated from Tauc plots using the absorbance data vs carrier concentration. (b) Theoretical Fermi level with respect to the valence band vs carrier concentration. Comparing energy differences at the same experimental carrier concentrations values yield $\Delta E$ values of 0.65 and 0.48 eV from the absorbance data and the theoretical calculations, respectively. Effective mass, $m^*$, and lattice perturbation constant, $\mu_0$, values used in the Fermi level calculation are the average of the range of the values found in literature.[32,49,56,57]

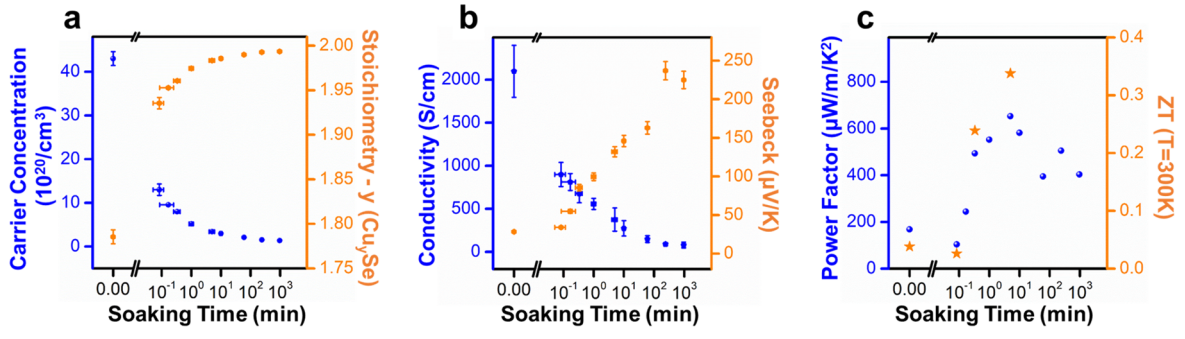


**Figure 6.** (a) Carrier concentration (blue) and stoichiometry (orange) estimations for $Cu_{2-x}Se$ samples prepared in this work as a function of soaking time in Cu ion solution. Increased soaking time leads to the decrease in carrier concentration as copper vacancies are filled. (b) TE parameter data for $Cu_{2-x}Se$ films prepared in this work: electrical conductivity (blue) and Seebeck coefficient (orange). The electrical conductivity and Seebeck coefficient trends are as predicted with the reduction of carrier concentration during the soaking process. (c) TE power factor (blue) and figure of merit, $ZT$ (orange), data as a function of Cu ion solution soaking time. Error bars are shown to depict the measurement uncertainty on a distinct sample. The optimal soaking time is about 6−7 min to achieve a maximum power factor of 653 $\mu$W/(m $K_2$) and a $ZT$ value of about 0.34, which are both the highest reported for a solution processed $Cu_2Se$ thin film known to-date.

interband excitation peak shifts to lower energy (800−1600 nm) and the broad intraband excitation peak slowly vanishes as the stoichiometry ratio is improved to 2:1 and vacancies are filled.

While qualitatively the trend is what one would expect, we proceeded further to test our optical data with the actual stoichiometry of the samples analyzed. We chose a range of stoichiometries including $Cu_{1.9}Se$, $Cu_{1.963}Se$, and $Cu_{1.995}Se$ to estimate the direct and indirect band gaps from a Tauc plot (Figures S4 and S5). The direct band gaps are plotted as a function of the carrier concentration (Figure 5a) and observe a

reduction of nearly 0.65 eV in optical band gap with increasing stoichiometry from $Cu_{1.9}Se$ to $Cu_{1.995}Se$. Similar to Figure 1, we can also simulate the carrier concentration as a function of the chemical potential. In Figure 5b, we demonstrate that using carrier concentration values for the $Cu_{1.9}Se$ and $Cu_{1.995}Se$ samples, the modeled chemical potential changes by 0.48 eV corresponding to a 0.48 eV reduction in the apparent optical band gap which is in casual agreement with the optical data. While the numbers (0.48 and 0.65 eV) do not match exactly, it should be noted that this change in stoichiometry also results in a change in crystal structure and hence, most likely a change in the band structure and band edges as well.

Our optical and structural data establish that when Cu deficient $Cu_{2-x}Se$ samples are soaked in a solution of Cu ions, empty states in the valence band are filled and the more structured $\alpha$-phase becomes dominant at room temperature as stoichiometry approaches $Cu_2Se$. This results in fewer hole carriers and drives the carrier concentration toward its optimal value for TE performance. Figure 6a clearly relates soaking time with stoichiometry and carrier concentration.

Stoichiometry was estimated from the average of 5−10 Hall carrier concentration readings assuming that a change in carrier concentration corresponds to a linear change in Cu vacancies.[21,52] With increasing soaking time, the stoichiometry increases toward $Cu_2Se$ along with a subsequent order of magnitude reduction in carrier concentration. The reduction of carrier concentration should improve TE properties toward the theoretical maximum $ZT$ of 1.69 (Figure 1).[32] Figure 6b shows measured in plane TE properties as a function of Cu ion solution soaking time. Electrical conductivity decreases with increased soaking time while the Seebeck coefficient increases, leading to an overall increase in TE power factor. This correlates with Boltzmann transport equation (BTE) TE physics where a decrease in carrier concentration often coincides with an increase in the Seebeck coefficient.[7] We used the single parabolic band theory to model the range of Seebeck coefficient and electrical conductivity values as a function of carrier concentration using literature parameters and find that our experimental values lie within this range (Figure S6 and details of the model in the SI). As the ratio of Cu:Se ratio approaches 2:1, we observe a change in the transport mechanism as well, demonstrated by our measurements of temperature dependent electrical conductivity (Figure S7). The electrical conductivity of a thin film with $Cu_{1.9}Se$ decreases with increasing temperature similar to the behavior of a degenerately doped semiconductor or a metal, while the electrical conductivity for the $Cu_{1.998}Se$ sample increases with increasing temperature akin to a semiconductor. The results are in agreement with our optical data that show intraband carrier absorption with $Cu_{1.9}Se$, proving that the Fermi level is deep within the valence band and classifying it as a degenerately doped semiconductor. As the sample is infused with more Cu ions rendering it closer to $Cu_2Se$, the Fermi level moves closer to the band edge, intraband absorption decreases and the material behaves like a semiconductor with decreased electrical conductivity.

Figure 6c shows the power factor and $ZT$ values based on the measured TE parameters as a function of soaking time. Values of $ZT$ are only presented for the samples for which cross-plane thermal conductivity was measured using time-domain thermoreflectance (details in the Thermal Conductivity Section in the SI). For thermal conductivity values, we assume that cross-plane thermal conductivity is a fair representation of in-plane thermal conductivity to align with the other in-plane measured TE parameters. In-plane thermal conductivity has historically been very challenging[71] to accurately measure and the relatively low values of thermal conductivity in our samples (<1 W/(m K)) would require a smaller beam that would further complicate the measurement. However, we acknowledge that if possible, measuring in-plane thermal conductivity would be the best practice to obtain the clearest representation of thermoelectric performance since the phonon scattering mechanism may be different based on the different interfaces that exist between the cross-plane and in-plane directions. Nevertheless, we still believe our assumption is fairly reasonable since our thin film is composed of similar sized nanoparticles distributed equally in all directions based on our SEM images in Figure 2. As predicted, TE performance is enhanced with the reduction of Cu vacancies and an optimal soaking time before the point of diminishing returns is seen to occur between 5 and 10 min. Our optimal power factor occurs at a value of about 650 $\mu W/(m\ K^2)$ when the $Cu_2Se$ films are soaked with Cu ions for around 6−7 min which is a 3−4-fold increase compared to recently reported power factor values at room temperature for $Cu_2Se$ thin films prepared via the thiol-amine dissolution process.[11,12,51]

With the performance of $Cu_2Se$ TE materials rapidly advancing toward commercial viability, the stability of the material needs to be addressed.[42,72] Figure S11 shows the results of a 22 h stability test consisting of testing the Seebeck coefficient for 100 repetitions allowing a 5 min cool-down period between measurements. The results show a 0.67 $\mu$V/K per hour reduction in the Seebeck coefficient during thermal cycling which raises stability concerns even at room temperature. However, many recent reports discuss and demonstrate improvements to the stability of $Cu_2Se$ at high temperatures, which leads us to believe that, using our facile ion impregnation approach, we can implement similar strategies to potentially alleviate these stability concerns during lower temperature operation.[41,44,73]

## CONCLUSIONS

In summary, we have significantly improved the room temperature power factor of $Cu_2Se$ thin films prepared by the thiol-amine dissolution process by a post treatment process which involves simply soaking the films in a solution of Cu ions for a brief 5−10 min. The result is a truly scalable and low-cost fabrication process which yields the highest TE power factor of 653 $\mu W/(m\ K^2)$ reported for a solution processed $Cu_2Se$ film to date. We demonstrated a reduction in the carrier concentration of $Cu_2Se$ from $4.3 \times 10^{21}$ to $3.4 \times 10^{20}$ $1/cm^3$. If the carrier concentration can be reduced even further to $4 \times 10^{19}$ $1/cm^3$ by alternate strategies that include elemental doping, alloying and energy filtering, it might be possible to achieve a $ZT$ of 1.69 at room temperature, where degradation issues of $Cu_2Se$ can potentially be mitigated. If achieved, $Cu_2Se$ can become an economical competitor for p-type materials in large scale TE applications and address the global need for sustainable and environmentally friendly solid-state cooling or power generation for microelectronics.

## EXPERIMENTAL METHODS

Two hundred milligrams of bulk $Cu_2Se$ powder was dissolved in a solution of 2 mL of ethylenediamine and 0.2 mL of ethane dithiol using a magnetic stirring hot plate. After filtration, fully dissolved $Cu_2Se$ solution was spin coated onto glass substrates at an RPM of 1800 for 60 s. The thin films were then annealed for 1 h at 350 °C. To perform the soaking process, $Cu_2Se$ thin films were soaked in a Cu ion solution in

acetonitrile and then rinsed in pure acetonitrile before drying with mild heat on a hot plate. To characterize the morphology, structure, composition and optical properties on the $Cu_2Se$ thin films, we performed SEM (Zeiss Gemini Ultra-55 Analytical Field Emission), XRD (Bruker AXS D8 Discover GADDS), XPS (Versa Probe II), XAS (Beamline 8.0.1 of the Advanced Light Source (ALS) in Berkeley, CA), and UV−vis−NIR (ASD QualitySpec Pro). Electrical measurements were performed via the standard 4 probe van-der-Pauw method and Seebeck measurements were performed on a homemade setup using small Peltier units (Ferrotec) to provide various temperature gradients. A LabView program was used with Keithley 2400 Sourcemeters and Agilent 34401 multimeters to provide current sources and measure voltages, respectively. Hall carrier concentrations were also obtained using an Ecopia HMS-5000 variable temperature Hall effect measurement system. Thermal conductivity measurements were performed using the standard time domain thermoreflectance (TDTR) method. Film thickness measurements were performed via a Veeco Dektak 150 profilometer and cross sectional SEM to accurately calculate electrical and thermal conductivities respectfully. Full details about experimental methods can be found in the Supporting Information along with supporting figures.

## AUTHOR INFORMATION


### Corresponding Authors

*E-mail: jjurban@lbl.gov.
*E-mail: asahu@nyu.edu.

### ORCID

Jinghua Guo: 0000-0002-8576-2172
Jeffrey J. Urban: 0000-0002-6520-830X
Ayaskanta Sahu: 0000-0002-1508-0213


### Notes

The authors declare no competing financial interest.

## ACKNOWLEDGMENTS


A.S. and M.R.S. thank the Tandon School of Engineering at New York University for financial support through start-up funds. This work was partially performed at the Molecular Foundry, Lawrence Berkeley National Laboratory along with the Advanced Light Source and was supported by the Department of Energy, Office of Science, Office of Basic Energy Sciences, Scientific User Facilities Division of the U.S. Department of Energy under Contract No. DE-AC02-05CH11231. E.Z. and M.P.G. gratefully acknowledge the National Science Foundation for fellowship support under the National Science Foundation Graduate Research Fellowship Program. We also gratefully acknowledge support for instrument use, scientific and technical assistance from the NYU Shared Instrumentation Facility through the Materials Research Science and Engineering Center (MRSEC) and MRI programs of the National Science Foundation under Award numbers DMR-1420073 and DMR-0923251, the Imaging and Surface Science Facilities of Advanced Science Research Center at the Graduate Center of CUNY, and FY's start-up support from the Stevens Institute of Technology. Finally, M.R.S. would like to thank the National Science Foundation for support under Award 1809064.


## REFERENCES


(1) Li, Z.; Xiao, C.; Zhu, H.; Xie, Y. Defect Chemistry for Thermoelectric Materials. *J. Am. Chem. Soc.* **2016**, *138*, 14810−14819.
(2) Yang, J.; Yip, H.-L.; Jen, A. K.-Y. Rational Design of Advanced Thermoelectric Materials. *Adv. Energy Mater.* **2013**, *3*, 549−565.
(3) Shi, X.; Chen, L.; Uher, C. Recent Advances in High-Performance Bulk Thermoelectric Materials. *Int. Mater. Rev.* **2016**, *61*, 379−415.
(4) Tan, G.; Zhao, L. D.; Kanatzidis, M. G. Rationally Designing High-Performance Bulk Thermoelectric Materials. *Chem. Rev.* **2016**, *116*, 12123−12149.
(5) Zeier, W. G.; Zevalkink, A.; Gibbs, Z. M.; Hautier, G.; Kanatzidis, M. G.; Snyder, G. J. Thinking Like a Chemist: Intuition in Thermoelectric Materials. *Angew. Chem., Int. Ed.* **2016**, *55*, 6826−6841.
(6) Yang, J.; Xi, L.; Qiu, W.; Wu, L.; Shi, X.; Chen, L.; Yang, J.; Zhang, W.; Uher, C.; Singh, D. J. On the Tuning of Electrical and Thermal Transport in Thermoelectrics: An Integrated Theory−experiment Perspective. *NPJ. Comput. Mater.* **2016**, *2*, 15015−15031.
(7) Rowe, D. M. *Thermoelectric Handbook: Macro to Nano*; CRC Press, 2005; pp 56−62.
(8) Bell, L. E. Cooling, Heating, Generating Power, and Recovering Waste Heat with Thermoelectric Systems. *Science* **2008**, *321*, 1457−1461.
(9) Sootsman, J. R.; Chung, D. Y.; Kanatzidis, M. G. New and Old Concepts in Thermoelectric Materials. *Angew. Chem., Int. Ed.* **2009**, *48*, 8616−8639.
(10) Zebarjadi, M.; Esfarjani, K.; Dresselhaus, M. S.; Ren, Z. F.; Chen, G. Perspectives on Thermoelectrics: From Fundamentals to Device Applications. *Energy Environ. Sci.* **2012**, *5*, 5147−5162.
(11) Lin, Z.; Hollar, C.; Kang, J. S.; Yin, A.; Wang, Y.; Shiu, H. Y.; Huang, Y.; Hu, Y.; Zhang, Y.; Duan, X. A Solution Processable High-Performance Thermoelectric Copper Selenide Thin Film. *Adv. Mater.* **2017**, *29*, 1606662.
(12) Ma, Y.; Vartak, P. B.; Nagaraj, P.; Wang, R. Y. Thermoelectric Properties of Copper Chalcogenide Alloys Deposited via the Solution-Phase Using a Thiol−amine Solvent Mixture. *RSC Adv.* **2016**, *6*, 99905−99913.
(13) Suarez, F.; Nozariasbmarz, A.; Vashaee, D.; Öztürk, M. C. Designing Thermoelectric Generators for Self-Powered Wearable Electronics. *Energy Environ. Sci.* **2016**, *9*, 2099−2113.
(14) Bahk, J.-H.; Fang, H.; Yazawa, K.; Shakouri, A. Flexible Thermoelectric Materials and Device Optimization for Wearable Energy Harvesting. *J. Mater. Chem. C* **2015**, *3*, 10362−10374.
(15) Chen, Y.; Zhao, Y.; Liang, Z. Solution Processed Organic Thermoelectrics: Towards Flexible Thermoelectric Modules. *Energy Environ. Sci.* **2015**, *8*, 401−422.
(16) Yang, Y.; Lin, Z. H.; Hou, T.; Zhang, F.; Wang, Z. L. Nanowire-Composite Based Flexible Thermoelectric Nanogenerators and Self-Powered Temperature Sensors. *Nano Res.* **2012**, *5*, 888−895.
(17) Im, H.; Moon, H. G.; Lee, J. S.; Chung, I. Y.; Kang, T. J.; Kim, Y. H. Flexible Thermocells for Utilization of Body Heat. *Nano Res.* **2014**, *7*, 443.
(18) Liu, X.; Long, Y. Z.; Liao, L.; Duan, X.; Fan, Z. Large-Scale Integration of Semiconductor Nanowires for High-Performance Flexible Electronics. *ACS Nano* **2012**, *6*, 1888−1900.
(19) Liu, H.; Shi, X.; Xu, F.; Zhang, L.; Zhang, W.; Chen, L.; Li, Q.; Uher, C.; Day, T.; Snyder, G. J. Copper Ion Liquid-like Thermoelectrics. *Nat. Mater.* **2012**, *11*, 422−425.
(20) Zhao, K.; Blichfeld, A. B.; Chen, H.; Song, Q.; Zhang, T.; Zhu, C.; Ren, D.; Hanus, R.; Qiu, P.; Iversen, B. B.; Xu, F.; Snyder, G. J.; Shi, X.; Chen, L. Enhanced Thermoelectric Performance through Tuning Bonding Energy in $Cu_2Se_{1-x}S_x$ Liquid-like Materials. *Chem. Mater.* **2017**, *29*, 6367−6377.
(21) Forster, J. D.; Lynch, J. J.; Coates, N. E.; Liu, J.; Jang, H.; Zaia, E.; Gordon, M. P.; Szybowski, M.; Sahu, A.; Cahill, D. G.; Urban, J. J. Solution-Processed $Cu_2Se$ Nanocrystal Films with Bulk-Like Thermoelectric Performance. *Sci. Rep.* **2017**, *7*, 2765−2771.

(22) Yang, H.; Bahk, J. H.; Day, T.; Mohammed, A. M. S.; Snyder, G. J.; Shakouri, A.; Wu, Y. Enhanced Thermoelectric Properties in Bulk Nanowire Heterostructure-Based Nanocomposites through Minority Carrier Blocking. *Nano Lett.* **2015**, *15*, 1349−1355.
(23) Zhang, Y.; Stucky, G. D. Heterostructured Approaches to Efficient Thermoelectric Materials. *Chem. Mater.* **2014**, *26*, 837−848.
(24) Harman, T. C.; Taylor, P. J.; Walsh, M. P.; Laforge, B. E.; Harman, T. C.; Taylor, P. J.; Walsh, M. P.; Laforge, B. E. Quantum Dot Superlattice Thermoelectric Materials and Devices. *Science* **2002**, *297*, 2229−2232.
(25) Fan, F. J.; Yu, B.; Wang, Y. X.; Zhu, Y. L.; Liu, X. J.; Yu, S. H.; Ren, Z. Colloidal Synthesis of $Cu_2CdSnSe_4$ Nanocrystals and Hot-Pressing to Enhance the Thermoelectric Figure-of-Merit. *J. Am. Chem. Soc.* **2011**, *133*, 15910−15913.
(26) Fang, H.; Bahk, J. H.; Feng, T.; Cheng, Z.; Mohammed, A. M. S.; Wang, X.; Ruan, X.; Shakouri, A.; Wu, Y. Thermoelectric Properties of Solution-Synthesized n-Type $Bi_2Te_3$ Nanocomposites Modulated by Se: An Experimental and Theoretical Study. *Nano Res.* **2016**, *9*, 117−127.
(27) Zhang, A.; Zhang, B.; Lu, W.; Xie, D.; Ou, H.; Han, X.; Dai, J.; Lu, X.; Han, G.; Wang, G.; Zhou, X. Twin Engineering in Solution-Synthesized Nonstoichiometric $Cu_5FeS_4$ Icosahedral Nanoparticles for Enhanced Thermoelectric Performance. *Adv. Funct. Mater.* **2018**, *28*, 1705117.
(28) Yin, D.; Liu, Y.; Dun, C.; Carroll, D. L.; Swihart, M. T. Controllable Colloidal Synthesis of Anisotropic Tin Dichalcogenide Nanocrystals for Thin Film Thermoelectrics. *Nanoscale* **2018**, *10*, 2533−2541.
(29) Park, S. H.; Jo, S.; Kwon, B.; Kim, F.; Ban, H. W.; Lee, J. E.; Gu, D. H.; Lee, S. H.; Hwang, Y.; Kim, J.-S.; Hyun, D.-B.; Lee, S.; Choi, K. J.; Jo, W.; Son, J. S. High-Performance Shape-Engineerable Thermoelectric Painting. *Nat. Commun.* **2016**, *7*, 13403−13412.
(30) Kim, J.; Lee, K. H.; Kim, S.-D.; Lim, J.; Myung, N. V. Simple and Effective Fabrication of $Sb_2Te_3$ Films Embedded with $Ag_2Te$ Nanoprecipitates for Enhanced Thermoelectric Performance. *J. Mater. Chem. A* **2018**, *6*, 349−356.
(31) Chen, B.; Das, S. R.; Zheng, W.; Zhu, B.; Xu, B.; Hong, S.; Sun, C.; Wang, X.; Wu, Y.; Claussen, J. C. Inkjet Printing of Single-Crystalline $Bi_2Te_3$ Thermoelectric Nanowire Networks. *Adv. Electron. Mater.* **2017**, *3*, 1600524−1600530.
(32) Day, T. W.; Weldert, K. S.; Zeier, W. G.; Chen, B. R.; Moffitt, S. L.; Weis, U.; Jochum, K. P.; Panthöfer, M.; Bedzyk, M. J.; Snyder, G. J.; Tremel, W. Influence of Compensating Defect Formation on the Doping Efficiency and Thermoelectric Properties of $Cu_{2-y}Se_{1-x}Br_x$. *Chem. Mater.* **2015**, *27*, 7018−7027.
(33) Brown, D. R.; Day, T.; Borup, K. A.; Christensen, S.; Iversen, B. B.; Snyder, G. J. Phase Transition Enhanced Thermoelectric Figure-of-Merit in Copper Chalcogenides. *APL Mater.* **2013**, *1*, 052107−052116.
(34) Qiu, P.; Shi, X.; Chen, L. Cu-Based Thermoelectric Materials. *Energy Storage Mater.* **2016**, *3*, 85−97.
(35) Yang, L.; Chen, Z. G.; Han, G.; Hong, M.; Zou, Y.; Zou, J. High-Performance Thermoelectric $Cu_2Se$ Nanoplates through Nanostructure Engineering. *Nano Energy* **2015**, *16*, 367−374.
(36) Bulat, L. P.; Osvenskii, V. B.; Ivanov, A. A.; Sorokin, A. I.; Pshenay-Severin, D. A.; Bublik, V. T.; Tabachkova, N. Y.; Panchenko, V. P.; Lavrentev, M. G. Experimental and Theoretical Study of the Thermoelectric Properties of Copper Selenide. *Semiconductors* **2017**, *51*, 854−857.
(37) Ballikaya, S.; Chi, H.; Salvador, J. R.; Uher, C. Thermoelectric Properties of Ag-Doped $Cu_2Se$ and $Cu_2Te$. *J. Mater. Chem. A* **2013**, *1*, 12478−12484.
(38) Zhao, L.; Wang, X.; Wang, J.; Cheng, Z.; Dou, S.; Wang, J.; Liu, L. Superior Intrinsic Thermoelectric Performance with ZT of 1.8 in Single-Crystal and Melt-Quenched Highly Dense $Cu_{2-x}Se$ Bulks. *Sci. Rep.* **2015**, *5*, 7671−7676.
(39) Pletcher, R. H.; Tannehill, J. C.; Anderson, D. A. *Computational Fluid Mechanics and Heat Transfer*; CRC Press: Boca Raton, FL, 1984; pp 255−258.
(40) Yang, D.; Su, X.; Yan, Y.; He, J.; Uher, C.; Tang, X. Mechanochemical Synthesis of High Thermoelectric Performance Bulk $Cu_2X$ (X = S, Se) Materials. *APL Mater.* **2016**, *4*, 116110−11617.
(41) Bailey, T. P.; Hui, S.; Xie, H. Y.; Olvera, A.; Poudeu, P. F. P.; Tang, X. F.; Uher, C. Enhanced ZT and Attempts to Chemically Stabilize $Cu_2Se$ via Sn Doping. *J. Mater. Chem. A* **2016**, *4*, 17225−17235.
(42) Dennler, G.; Chmielowski, R.; Jacob, S.; Capet, F.; Roussel, P.; Zastrow, S.; Nielsch, K.; Opahle, I.; Madsen, G. K. H. Are Binary Copper Sulfides/Selenides Really New and Promising Thermoelectric Materials? *Adv. Energy Mater.* **2014**, *4*, 1301581.
(43) Beretta, D.; Neophytou, N.; Hodges, J. M.; Kanatzidis, M. G.; Narducci, D.; Martin- Gonzalez, M.; Beekman, M.; Balke, B.; Cerretti, G.; Tremel, W.; Zevalkink, A.; Hofmann, A. I.; Müller, C.; Dörling, B.; Campoy-Quiles, M.; Caironi, M. Thermoelectrics: From History, a Window to the Future. *Mater. Sci. Eng., R* **2018**, DOI: 10.1016/j.mser.2018.09.001.
(44) Olvera, A. A.; Moroz, N. A.; Sahoo, P.; Ren, P.; Bailey, T. P.; Page, A. A.; Uher, C.; Poudeu, P. F. P. Partial Indium Solubility Induces Chemical Stability and Colossal Thermoelectric Figure of Merit in $Cu_2Se$. *Energy Environ. Sci.* **2017**, *10*, 1668−1676.
(45) Bob, B.; Lei, B.; Chung, C.-H.; Yang, W.; Hsu, W.-C.; Duan, H.-S.; Hou, W. W.-J.; Li, S.-H.; Yang, Y. The Development of Hydrazine-Processed $Cu(In,Ga)(Se,S)_2$ Solar Cells. *Adv. Energy Mater.* **2012**, *2*, 504−522.
(46) Dolzhnikov, D. S.; Zhang, H.; Jang, J.; Son, J. S.; Panthani, M. G.; Shibata, T.; Chattopadhyay, S.; Talapin, D. V. Composition-Matched Molecular " Solders " for Semiconductors. *Science* **2015**, *347*, 425.
(47) Mitzi, D. B.; Kosbar, L. L.; Murray, C. E.; Copel, M.; Afzali, A. High-Mobility Ultrathin Semiconducting Films Prepared by Spin Coating. *Nature* **2004**, *428*, 299−303.
(48) Zhang, H.; Son, J. S.; Dolzhnikov, D. S.; Filatov, A. S.; Hazarika, A.; Wang, Y.; Hudson, M. H.; Sun, C. J.; Chattopadhyay, S.; Talapin, D. V. Soluble Lead and Bismuth Chalcogenidometallates: Versatile Solders for Thermoelectric Materials. *Chem. Mater.* **2017**, *29*, 6396−6404.
(49) Lin, Z.; He, Q.; Yin, A.; Xu, Y.; Wang, C.; Ding, M.; Cheng, H. C.; Papandrea, B.; Huang, Y.; Duan, X. Cosolvent Approach for Solution-Processable Electronic Thin Films. *ACS Nano* **2015**, *9*, 4398−4405.
(50) McCarthy, C. L.; Webber, D. H.; Schueller, E. C.; Brutchey, R. L. Solution-Phase Conversion of Bulk Metal Oxides to Metal Chalcogenides Using a Simple Thiol-Amine Solvent Mixture. *Angew. Chem., Int. Ed.* **2015**, *54*, 8378−8381.
(51) Webber, D. H.; Brutchey, R. L. Alkahest for $V_2VI_3$ Chalcogenides: Dissolution of Nine Bulk Semiconductors in a Diamine-Dithiol Solvent Mixture. *J. Am. Chem. Soc.* **2013**, *135*, 15722−15725.
(52) Kang, S. D.; Danilkin, S. A.; Aydemir, U.; Avdeev, M.; Studer, A.; Snyder, G. J. Apparent Critical Phenomena in the Superionic Phase Transition of $Cu_{2-x}Se$. *New J. Phys.* **2016**, *18*, 013024.
(53) Mi, W.; Qiu, P.; Zhang, T.; Lv, Y.; Shi, X.; Chen, L. Thermoelectric Transport of Se-Rich $Ag_2Se$ in Normal Phases and Phase Transitions. *Appl. Phys. Lett.* **2014**, *104*, 133903.
(54) He, Y.; Day, T.; Zhang, T.; Liu, H.; Shi, X.; Chen, L.; Snyder, G. J. High Thermoelectric Performance in Non-Toxic Earth-Abundant Copper Sulfide. *Adv. Mater.* **2014**, *26*, 3974−3978.
(55) Finefrock, S. W.; Yang, H.; Fang, H.; Wu, Y. Thermoelectric Properties of Solution Synthesized Nanostructured Materials. *Annu. Rev. Chem. Biomol. Eng.* **2015**, *6*, 247−266.
(56) Lv, Y.; Chen, J.; Zheng, R. K.; Shi, X.; Song, J.; Zhang, T.; Li, X.; Chen, L. (001)-Oriented $Cu_{2-y}Se$ Thin Films with Tunable Thermoelectric Performances Grown by Pulsed Laser Deposition. *Ceram. Int.* **2015**, *41*, 7439−7445.
(57) Gorbachev, V. V.; Putilin, I. M. Some Parameters of Band Structure in Copper Selenide and Telluride. *Phys. Status Solidi* **1973**, *16*, 553−559.
(58) Yang, L.; Chen, Z. G.; Han, G.; Hong, M.; Zou, J. Impacts of Cu Deficiency on the Thermoelectric Properties of $Cu_{2-x}Se$ Nanoplates. *Acta Mater.* **2016**, *113*, 140−146.

(59) Lesnyak, V.; Brescia, R.; Messina, G. C.; Manna, L. Cu Vacancies Boost Cation Exchange Reactions in Copper Selenide Nanocrystals. *J. Am. Chem. Soc.* **2015**, *137*, 9315−9323.
(60) Xie, Y.; Riedinger, A.; Prato, M.; Casu, A.; Genovese, A.; Guardia, P.; Sottini, S.; Sangregorio, C.; Miszta, K.; Ghosh, S.; Pellegrino, T.; Manna, L. Copper Sulfide Nanocrystals with Tunable Composition by Reduction of Covellite Nanocrystals with $Cu^{+}$ ions. *J. Am. Chem. Soc.* **2013**, *135*, 17630−17637.
(61) Dorfs, D.; Härtling, T.; Miszta, K.; Bigall, N. C.; Kim, M. R.; Genovese, A.; Falqui, A.; Povia, M.; Manna, L. Reversible Tunability of the Near-Infrared Valence Band Plasmon Resonance in $Cu_{2-x}Se$ Nanocrystals. *J. Am. Chem. Soc.* **2011**, *133*, 11175−11180.
(62) Kundu, B.; Bera, A.; Pal, A. J. Differential Conductance (d I / d V) Imaging of a Heterojunction-Nanorod. *Nanotechnology* **2017**, *28*, 095705.
(63) Zaia, E. W.; Sahu, A.; Zhou, P.; Gordon, M. P.; Forster, J. D.; Aloni, S.; Liu, Y. S.; Guo, J.; Urban, J. J. Carrier Scattering at Alloy Nanointerfaces Enhances Power Factor in PEDOT:PSS Hybrid Thermoelectrics. *Nano Lett.* **2016**, *16*, 3352−3359.
(64) Lyubinetsky, I.; El-Azab, A.; Lea, A. S.; Thevuthasan, S.; Baer, D. R. Initial Stages of Oxide Nanodot Heteroepitaxial Growth: $Cu_2O$ on $SrTiO_3$(100). *Appl. Phys. Lett.* **2004**, *85*, 4481−4483.
(65) Mahan, G. D. The Seebeck Coefficient of Superionic Conductors. *J. Appl. Phys.* **2015**, *117*, 045101.
(66) Sirusi, A. A.; Ballikaya, S.; Uher, C.; Ross, J. H. Low-Temperature Structure and Dynamics in $Cu_2Se$. *J. Phys. Chem. C* **2015**, *119*, 20293−20298.
(67) Sun, Y.; Xi, L.; Yang, J.; Wu, L.; Shi, X.; Chen, L.; Snyder, J.; Yang, J.; Zhang, W. The ″Electron Crystal″ Behavior in Copper Chalcogenides $Cu_2X$ (X = Se, S). *J. Mater. Chem. A* **2017**, *5*, 5098−5105.
(68) Lu, P.; Liu, H.; Yuan, X.; Xu, F.; Shi, X.; Zhao, K.; Qiu, W.; Zhang, W.; Chen, L. Multiformity and Fluctuation of Cu Ordering in $Cu_2Se$ Thermoelectric Materials. *J. Mater. Chem. A* **2015**, *3*, 6901−6908.
(69) Garba, E. J. D.; Jacobs, R. L. The Electronic Structure of $Cu_{2-x}Se$. *Physica B+C* **1986**, *138*, 253−260.
(70) Gulay, L.; Daszkiewicz, M.; Strok, O.; Pietraszko, A. Crystal Structure of $Cu_2Se$. *Chem. Met. Alloy.* **2011**, *4*, 200−205.
(71) Feser, J. P.; Liu, J.; Cahill, D. G. Pump-Probe Measurements of the Thermal Conductivity Tensor for Materials Lacking in-Plane Symmetry. *Rev. Sci. Instrum.* **2014**, *85*, 104903−104911.
(72) Brown, D. R.; Day, T.; Caillat, T.; Snyder, G. J. Chemical Stability of $(Ag,Cu)_2Se$: A Historical Overview. *J. Electron. Mater.* **2013**, *42*, 2014−2019.
(73) Kang, S. D.; Pöhls, J.-H.; Aydemir, U.; Qiu, P.; Stoumpos, C. C.; Hanus, R.; White, M. A.; Shi, X.; Chen, L.; Kanatzidis, M. G.; Snyder, G. J. Enhanced Stability and Thermoelectric Figure-of-Merit in Copper Selenide by Lithium Doping. *Mater. Today Phys.* **2017**, *1*, 7−13.